Eur Biophys J (2009) 38:813–828
DOI 10.1007/s00249-009-0499-9

ORIGINAL PAPER

Analysis of protein mobilities and interactions in living cells by multifocal fluorescence fluctuation microscopy

Gerrit Heuvelman · Fabian Erdel · Malte Wachsmuth · Karsten Rippe

Received: 3 March 2009 / Revised: 24 May 2009 / Accepted: 25 May 2009 / Published online: 19 June 2009

Abstract The spatial and temporal fluctuation microscope (STFM) presented here extends the concept of a fluorescence confocal laser scanning microscope to illumination and detection along a line. The parallel multichannel acquisition of the fluorescence signal was accomplished by using a single line of an electron-multiplying charge-coupled device camera at 14 μs time resolution for detection of the fluorescence signal. The STFM system provided fast confocal imaging (30 images per second) and allowed for the spatially resolved detection of particle concentration fluctuations in fluorescence correlation spectroscopy experiments. For the application of the STFM, an approximated theoretical description of the beam geometry, the point-spread function, and the fluorescence auto- and cross-correlation functions were derived. The STFM was applied to studies of the dynamics of promyelocytic leukemia nuclear bodies, green fluorescent protein, and chromatin-remodeling complexes in living cells. The results demonstrate the unique capabilities of the STFM for characterizing the position-dependent translocations and interactions of proteins in the cell.

Keywords Fluorescence correlation spectroscopy · Single-particle tracking · Promyelocytic leukemia nuclear body · Green fluorescent protein · Chromatin-remodeling complex · Protein dynamics in living cells

Abbreviations

GFP	Green fluorescent protein
MSD	Mean-squared displacement
SPT	Single-particle tracking
FRAP	Fluorescence recovery after photobleaching
FCS	Fluorescence correlation spectroscopy
FCCS	Fluorescence cross-correlation spectroscopy
STFM	Spatial and temporal fluctuation microscope/ microscopy
CLSM	Fluorescence confocal laser-scanning microscope
EM-CCD	Electron-multiplying charge-coupled device
PML-NB	Promyelocytic leukemia nuclear body
PSF	Point-spread function
TIRF	Total internal reflection fluorescence

This article has been submitted as a contribution to the festschrift entitled "Uncovering cellular sub-structures by light microscopy" in honour of Professor Cremer's 65th birthday.

G. Heuvelman · F. Erdel · K. Rippe (✉)
Research Group Genome Organization and Function, Deutsches Krebsforschungszentrum and BioQuant, Im Neuenheimer Feld 280, 69120 Heidelberg, Germany
e-mail: Karsten.Rippe@bioquant.uni-heidelberg.de; Karsten.Rippe@DKFZ-Heidelberg.de

M. Wachsmuth (✉)
Cell Biology and Biophysics Unit, European Molecular Biology Laboratory, Meyerhofstr. 1, 69117 Heidelberg, Germany
e-mail: M.Wachsmuth@embl.de

Introduction

The mobilities of proteins, nucleic acids, and their complexes inside living cells can be studied using a number of fluorescence microscopy-based techniques (Wachsmuth et al. 2008). These are frequently related to images of cellular structures from fluorescence confocal laser scanning microscopy (CLSM) to identify localization-specific dynamics and interactions of a fluorescently labeled species. The most direct determination of the movement of a particle is to follow its path in the cell on a series of images over time. This method is referred to as single-particle

tracking (SPT; Qian and Elson 1991). SPT requires sufficient fluorescence signal intensity to identify individual particles at a given temporal and spatial resolution, and to characterize their motion. Frequently, however, single fluorescent particles cannot be traced and the use of less direct techniques based on ensemble analysis is required. One group of such methods relies on the photo-induced bleaching (or activation) of marker molecules in selected areas of a cell and subsequent or simultaneous relaxation back to equilibrium. The most prominent representative of this approach is FRAP (fluorescence recovery after photobleaching) (Axelrod et al. 1976; Peters et al. 1974), with methods such as continuous fluorescence photobleaching (CP) or fluorescence loss in photobleaching (FLIP) being conceptionally related (Cole et al. 1996; Cutts et al. 1995; Peters et al. 1981; Wachsmuth et al. 2003). An alternative set of methods is referred to as fluorescence correlation spectroscopy (FCS), where single molecule properties can be identified and are averaged over a larger number of molecules. It employs thermal equilibrium fluctuations in order to determine diffusion properties and interactions (Elson and Magde 1974; Magde et al. 1972, 1974). In an FCS experiment, the focus of a confocal laser illumination and fluorescence-detection system such as that of a CLSM defines a small observation volume. It is fixed at a position of interest. Due to their diffusion, fluorescently labeled molecules can enter and leave the focus, resulting in signal fluctuations at the detector. The average lengths and amplitudes of the fluctuations are determined by a temporal autocorrelation analysis (Wachsmuth and Weisshart 2007). Appropriate biophysical models for the sources of fluctuations allow, for example, the quantification of the concentrations and diffusion coefficients and the discrimination of small free proteins from large complexes to which they are bound. Besides diffusion, other sources of fluctuations include photophysical effects such as molecular blinking/intermittence, interactions with cellular structures, or the movement of these structures themselves. In the simple and frequent case of freely mobile molecules, the major readouts of FCS are the number of molecules and their mean dwell time in the observation volume.

While the above-mentioned conventional type of FCS, especially in conjunction with CLSM imaging, provides a higher spatial and temporal resolution than FRAP, spatially differentiated data can be obtained only by sequential acquisition of point measurements at different positions and localizations in the cell. These can include the cytoplasm, the nucleus, the nucleolus, or any other subcompartments that can be identified on the CLSM images. In order to acquire spatially resolved maps of the particle dynamics by FCS, a number of approaches have been developed: (1) In a step-wise raster-scanning pattern, short intensity traces are collected at each pixel, from which correlation functions are calculated for each pixel (Kudryavtsev et al. 2007). As a drawback of this approach, the resulting curves are rather noisy and make it difficult to assess details of the diffusion process beyond the estimation of a diffusion coefficient. (2) Various combinations of beam scanning and spatio-temporal correlation spectroscopy have been implemented: For scanning FCS (sFCS), the fluorescence intensity trace is collected along the trajectory of an excitation laser beam that is directed continuously and rapidly in a uniform, often circular, scan in a repetitive fashion (Berland et al. 1996; Palmer and Thompson 1987; Petrasek and Schwille 2008; Ruan et al. 2004; Skinner et al. 2005). In order to provide accurate FCS data at every position of the beam trajectory, the scan rate needs to be fast compared to the diffusion of the particles. This approach benefits from reduced photobleaching compared to point measurements. However, spatially differentiated measurements are time-consuming and are therefore difficult to conduct in living cells since these display high dynamics of their organization. (3) While the above-mentioned approaches normally require custom-designed equipment, the raster image correlation spectroscopy (RICS) method is conceptually close to sFCS and employs conventional CLSM images for spatially resolved FCS measurements (Brown et al. 2008; Digman et al. 2005a, b; Kolin and Wiseman 2007). Since the CLSM is a raster-scan instrument, the image pixels are in a well-defined temporal and spatial relationship to one another. Thus, the data provide spatially resolved dynamics information in the microsecond to second time range (Digman et al. 2005b). Mobilities in the range of the pixel capture rate are determined by correlating intensities of neighboring pixels, which requires averaging over a sufficiently high number of pixels and hence leads to loss of spatial resolution. Slower mobilities are determined from successive images, so that each focal position is measured for only a fraction of the measurement time. Additionally, the photon yield of this method is rather low and the resulting effective spatial optical resolution is limited. (4) Imaging of molecular dynamics can be performed by parallelized FCS data acquisition using multifocal systems, which combine two-dimensional imaging and optical sectioning with FCS in one or more dimensions. Examples of this approach are double-focus FCS (dfFCS; Bayer and Radler 2006; Brinkmeier et al. 1997; Burkhardt and Schwille 2006; Hwang and Wohland 2007; Lumma et al. 2003; Pan et al. 2007), multifocal spinning disk FCS (Sisan et al. 2006), and total internal reflection fluorescence correlation microscopy (TIR-FCM; Kannan et al. 2007; Schwille 2003). The parallelized FCS measurements reduce the data acquisition time significantly. In dfFCS a modified FCS setup generates two excitation volumes in the probe typically separated by not more than a few micrometers with

corresponding data acquisition by two detectors. The limited number of only two simultaneous measurement positions is a disadvantage of this technique. The spinning disk FCS parallelizes the FCS measurement by using a spinning disk confocal microscope. This approach can spatially map diffusion coefficients or flow velocities at up to approximately 10 independent locations simultaneously (Sisan et al. 2006). However, the optical resolution is limited and the photon yield is relatively low. Finally, the TIR-FCM has been developed as a combination of TIRF and FCS. Currently, the time resolution of this system is 4 ms comprising 20 lines in the CCD with the restriction of the observation to 100 nm and less above the coverslip (Kannan et al. 2007).

In order to overcome the restrictions of the existing approaches, such as limited temporal and spatial resolution and/or long measurement times, a new method for spatially resolved mobility measurements in living cells termed spatial and temporal fluctuation microscopy (STFM) is introduced here. STFM extends the point confocal concept to illumination and detection volumes for FCS and imaging arranged along a line. It offers high three-dimensional spatial resolution to identify cellular structures as well as fast two- or three-dimensional time-lapse imaging for example for single particle tracking. In line-scanning imaging mode, the integration time per line/pixel can be increased compared to a point scanner while the image acquisition rate is the same or even faster than those obtained with a conventional CLSM. In this way, a much lower laser intensity per pixel is required with less photobleaching and higher photon yield compared to point scanning (Borlinghaus 2006). Furthermore, single-photon counting detection, i.e., detection at high quantum yield and high signal-to-noise ratio, with microsecond time resolution allows for spatially resolved parallel FCS measurements at hundreds of points along a line by using a single line of an EM-CCD camera. The capabilities of the STFM are demonstrated in vitro with fluorescent quantum dots as a reference and applied to studying the dynamics of three biological systems: promyelocytic leukemia nuclear bodies (PML-NBs), green fluorescent protein (GFP), and GFP-tagged chromatin-remodeling complexes of Snf2H protein in living cells. The results reveal fluctuations in protein mobility throughout the nucleus that have not been identified previously.

Materials and methods

Cell lines for live-cell fluorescence microscopy/spectroscopy analysis

PML-NBs were labeled via transiently transfecting cells of the human U2OS osteosarcoma cell line (HTB-96) with GFP-PML III as described previously (Jegou et al. 2009). Cells were grown in D-MEM medium (Invitrogen, CA, USA) containing 10% FCS (PAA, Austria). The analysis of GFP or Snf2H-GFP mobility was conducted in human HeLa cervical cancer cells or U2OS cells that were cultured in D-MEM medium supplemented with 10% FCS for 1 day after plating. Cells were transiently transfected with plasmid vectors for GFP (pEGFP-N1, Clontech, CA, USA) or Snf2H-GFP using Effectene (Qiagen, Hilden, Germany) according to standard protocols. After transfection, cells were cultured for 1 day before using them for imaging and FCS measurements. The plasmid pEGFP-N3-Snf2H was kindly provided by Patrick Varga-Weisz and contains the full coding sequence of human Snf2H fused to GFP at the C-terminus (Collins et al. 2002).

The spatial and temporal fluctuation microscope (STFM)

The spatial and temporal fluctuation microscope extends the point-confocal concept to multifocal illumination and detection along a line (Fig. 1; Heuvelman 2008). It consists of a custom-designed line-scanning laser illumination and fluorescence detection setup that is attached to an inverted Leica DM IRBE microscope equipped with a Leica UPlanApo 63x 1.2 NA water immersion lens with coverglass correction (Leica Microsystems, Germany). For fluorescence excitation, a fiber-coupled Coherent Sapphire DPSS laser emitting at 488 nm was used with an output power of 200 mW (Coherent, Germany). The line profile for illumination is generated with cylindrical lenses in the illumination beam path in such a way that in the intermediate image plane, between the scan and the tube lens, the laser light is focused to the diffraction limit in one direction (depicted as “top view” in Fig. 1) and collimated in the other direction (“side view” in Fig. 1). The microscope images this profile into the focal plane of the objective lens with the corresponding demagnification by a factor of 63. A dichroic mirror transmits the excitation light below 500 nm towards the sample and reflects the emitted fluorescence light towards a bandpass filter (500–550 nm) and the detector. A single-axis scan mirror rotary around an axis perpendicular to the plane of projection in the top view of Fig. 1 adjusts the vertical line position, whereas horizontal scanning is not necessary due to the line profile. Fluorescence from the illuminated line is imaged on a single line of an electron-multiplying charge-coupled device (EM-CCD; SamBa SE-34, Sensovation, Germany). Every pixel along this line of the EM-CCD serves as a point detector. A 25-µm-wide slit is positioned in a conjugate image plane in order to provide optical sectioning and to prevent fluorescence light from falling on any pixel of the EM-CCD chip lying outside the line. The

magnification from the probe to the slit is 126-fold so that the slit width corresponds to ~200 nm in the focal plane of the objective lens. On the other hand, the demagnification from the slit to the detector is 3.33-fold so that the slit width corresponds to the pixel size of 7.4 μm. Every pixel corresponds to 200 nm in the sample, close to the diffraction-limited resolution of the system (see "Results" section). Thus, in combination with line illumination, the fluorescence from hundreds of pixels along the line is detected simultaneously with good spatial resolution also along the optical axis. An acquisition rate of up to 70,000 lines per second (lps) was achieved (corresponding to a time resolution of 14 μs), which is one to two orders of magnitude faster than previous setups (Kannan et al. 2007).

In a conventional CLSM or FCS setup, the point-spread function (PSF) can be approximated by a three-dimensional Gaussian profile. In contrast, the PSF of the STFM is the product of the illumination profile, which is constant along the line and similar (though not equal) to the point illumination profile perpendicular to the line, and the detection profile, which corresponds to the point detection profile (Fig. 2a). A more detailed description of the PSF and the resulting correlation functions is given in the "Results" section. Perpendicular to the slit, the optical path resembles the point-confocal case adapted to a rectangular aperture. Parallel to the slit the characteristics are that of a wide-field epifluorescence setup. Thus, an image acquired with the STFM shares aspects from both setups: the axial resolution of 700 nm is better than in a wide-field microscope but worse than in a CLSM because the slit blocks less out-of-focus light than the confocal pinhole does, resulting in additional background (Pawley 1995) and possibly affecting the amplitude of the correlation function. Moreover, the slit leads to different resolutions along and perpendicular to the line amounting to 380 and 200 nm, respectively, as determined experimentally with fluorescent beads (Heuvelman 2008). A detailed description of the implementation and the characterization of the instrument's performance will be reported in detail elsewhere (Heuvelman et al., unpublished data). The STFM operates in two modes and is controlled by software written in Visual C++ (Microsoft, WA, USA). Images of 128 × 512 pixels can be acquired at a maximum rate of 100 frames per second (fps) to track particles or to visualize cellular structures. For this frame rate, however, in most cases the bleaching effect on the pool of fluorescent molecules due to the required high illumination intensity becomes very pronounced as bleaching a line inside a cellular structure has more impact than bleaching a point. On an acquired image a line can be chosen to collect FCS data, i.e., the intensity is recorded over time at every pixel along the line with a time resolution of 14 μs.

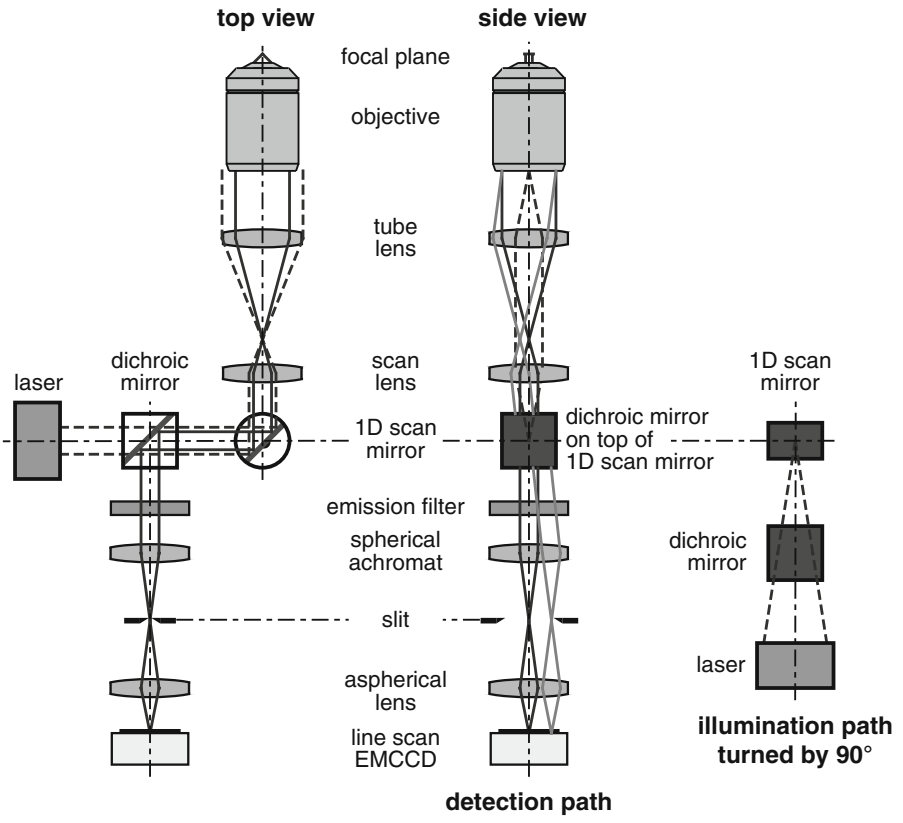

Fig. 1 Schematical representation of the spatial and temporal fluctuation microscope (STFM). A *top view* and a *side view* of the STFM line-scan setup are depicted. In the side view, the illumination path is turned by 90°. The *dashed lines* display the illumination beams and the *solid lines* the emission beams for a point in the middle (*dark gray*) and for a point at the edge of the illuminated line (*light gray*). As the scanning mirror only rotates around one axis, it is drawn as a scan mirror in the top view and as a fixed mirror in the side view

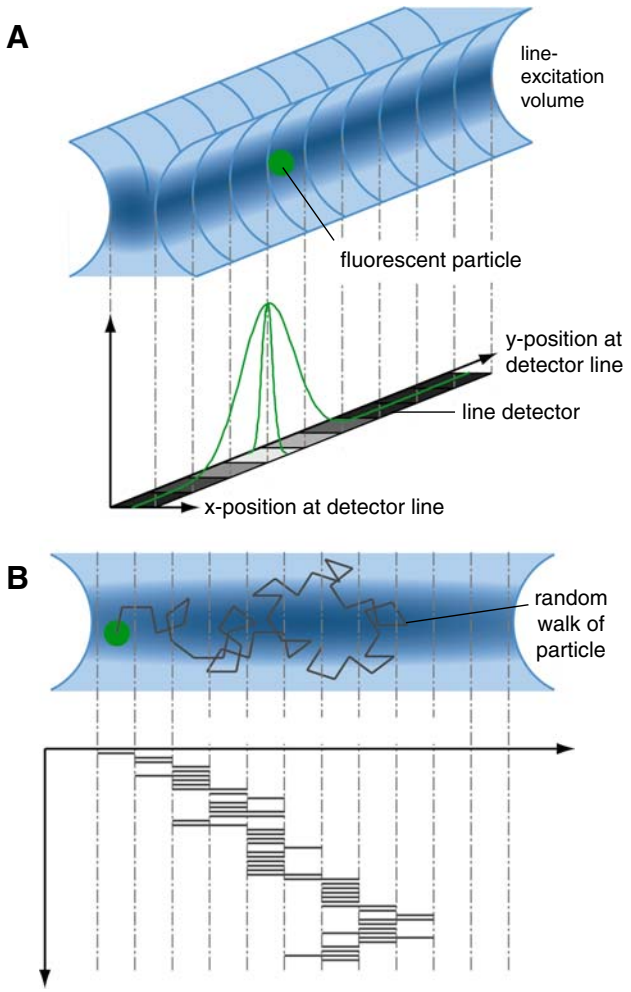

Fig. 2a, b Concept of data acquisition with the STFM. **a** The fluorescence originating from the line-shaped illumination volume is projected on a pixel line array of an EM-CCD camera. A fluorescently labeled particle in the illuminated volume gives rise to a Gaussian-shaped intensity profile on the line detector, which is described by the point-spread function. **b** The fluorescently labeled particle moves in, through, and out of the illuminated and detected line. This line is divided into several detection volumes corresponding to each pixel along the detector array. The particle movements will be detected as a series of short, randomized fluorescence signals at the corresponding pixel of the line detector

Fast imaging of PML-NBs

Using the fast-imaging feature of the STFM for the single-particle tracking of PML-NBs, images were acquired at 5.1 fps for an image size of 25 × 25 µm. This corresponds to an integration time per line/pixel of 1.5 ms. From the resulting images, the mean-squared displacement (MSD) was calculated for different time steps and averaged according to

$$\mathrm{MSD}(m) = \frac{1}{N-n+1}\sum_{n>m}^{N}\sqrt{(x_n - x_{n-m})^2 + (y_n - y_{n-m})^2} \quad (1)$$

In this equation, N is the total number of images, (x_n, y_n) the tracked position of the nuclear body in the n-th image, and m the time period in units of Δt, which is the time between subsequent images. To account for any translocations of the cell during the experiment, the mean-squared change in distance between two PML-NBs MSΔD was calculated as described previously (Jegou et al. 2009).

$$\mathrm{MS\Delta D}(m) = \frac{1}{N-n+1}\sum_{n>m}^{N}\sqrt{(d_n - d_{n-m})^2} \quad (2)$$

In Eq. 2, d_n is the distance between the tracked positions of two PML-NBs in image n. To elucidate the concept of the STFM one-dimensional time traces of slowly diffusing 100-nm beads, i.e., plain fluorescent polystyrene nanospheres (Corpuscular, NY, USA), at a concentration of 0.1 beads per µm^3 were imaged for 13 s with a line acquisition rate of 380 lps, corresponding to an integration time of 2.6 ms per pixel/line at a line width of 128 pixels or 25 µm.

Fluorescence correlation spectroscopy measurements with the STFM

In vitro FCS studies with the STFM were conducted with green-fluorescent quantum dot streptavidin conjugates (QDot525) with a size of ~15 nm (Invitrogen, Karlsruhe, Germany). Quantum dots provide high fluorescence brightness and photostability (Gomez et al. 2006; Heuff et al. 2007). However, due to their photophysical properties they exhibit a significant amount of blinking. This was accounted for by introducing an additional blinking term in the FCS autocorrelation fit function as described previously (Heuff et al. 2007). The quantum dots were recorded at about 38,900 lps for a total acquisition time of 60 s, corresponding to an integration time of ca. 26 µs per pixel/line at a line width of 128 pixels or 25 µm. The same data were also subject to auto- and cross-correlation analyses. The auto- and cross-correlation functions were calculated according to

$$G_{kl}(\tau) = \frac{\langle F_k(t)F_l(t+\tau)\rangle}{\langle F_k(t)\rangle\langle F_l(t)\rangle} - 1 \quad (3)$$

where F_k and F_l stand for the fluorescence signal in pixels k and l, respectively, and τ for the correlation lag time. The correlation functions were subsequently fitted to Eq. 8 (see "Results" section for a detailed description and derivation)

for the case of free diffusion using Origin (OriginLab, MA, USA).

For the experiments with GFP- and Snf2H-GFP-expressing cells, the integration times for the EM-CCD camera were set to 60 and to 115 μs, respectively. For both measurements, a total acquisition time of 60 s was used. The correlation functions for each pixel were calculated and fitted in the same way as described above. However, an anomalous diffusion model was applied by replacing τ/τ_{diff} with $(\tau/\tau_{\text{diff}})^{\alpha}$, with the diffusion correlation time τ_{diff} and the anomaly parameter α used as additional fit parameters.

CLSM imaging and point FCS of GFP and Snf2H-GFP

Confocal imaging and point FCS measurements were conducted using a Leica TCS SP2 AOBS FCS2 system (Leica Microsystems, Germany) equipped with a Leica UPlanApo 63× 1.2 NA water immersion lens with cover-glass correction. GFP was excited with the 488-nm line of an argon laser. The resulting correlation functions were calculated according to Eq. 3 and then fitted to the following expression (Wachsmuth et al. 2000):

$$G(\tau)=\frac{1}{cV_{\text{eff}}}[1-\Theta+\Theta\cdot e^{-\tau/\tau_{\text{trip}}}] \cdot\left[f_1\cdot\left(1+\left(\frac{\tau}{\tau_{\text{D1}}}\right)^{\alpha_1}\right)^{-1}\left(1+\frac{1}{\kappa^2}\left(\frac{\tau}{\tau_{\text{D1}}}\right)^{\alpha_1}\right)^{-1/2} +(1-f_1)\cdot\left(1+\left(\frac{\tau}{\tau_{\text{D2}}}\right)^{\alpha_2}\right)^{-1}\left(1+\frac{1}{\kappa^2}\left(\frac{\tau}{\tau_{\text{D2}}}\right)^{\alpha_2}\right)^{-1/2}\right] \tag{4}$$

This is the autocorrelation function for two anomalously diffusing species: c denotes the total particle concentration, $V_{\text{eff}}=\pi^{3/2}\kappa w_0^3$ the effective volume, κ the structure factor, i.e., the ratio of axial to lateral radius of the focal volume, ω_0 is the lateral focus radius, τ_{D1} and τ_{D2} the characteristic diffusion correlation times for the two species, α_1 and α_2 the anomaly parameters for the two species, and f_1 the fraction of the first species. Θ is the fraction of molecules in a non-fluorescent state and τ_{trip} the apparent lifetime in this state. The autocorrelation function for GFP was fitted with one species ($f_1 = 1$). In the case of Snf2H, two species were required since transient binding of Snf2H and chromatin led to the presence of diffusing chromatin structures that were associated with labeled Snf2H. Thus, the second species reflected chromatin motion, which was not further investigated in the present study. Diffusion coefficients were calculated from the measured diffusion times according to $D = \omega_0^2/4\tau_{\text{diff}}$. These are referred to in the text as "apparent" diffusion coefficients since they include contributions from transient binding of the particle and/or an anomalous diffusion behavior.

Results

Approximated analytical description of the STFM optical setup

In the context of FCS, the total PSF of a fluorescence imaging system is often referred to as molecular detection efficiency $\Psi(x, y, z)$. As fluorescence is an incoherent process, the PSF is simply the product of the illumination and the detection PSF and, in a scalar approximation, related to the respective field amplitude distributions according to

$$\begin{aligned}\Psi(x,y,z) &= \text{PSF}_{\text{ill}}(x,y,z)\cdot\text{PSF}_{\text{det}}(x,y,z)\\ &= |h_{\text{ill}}(x,y,z)|^2(|h_{\text{em}}(x,y,z)|^2 * S(x,y))\end{aligned} \tag{5}$$

where * denotes the convolution and $S(x, y)$ describes the effective detection area of the pixel behind the slit in the line-detection setup. The parameters h_{ill} and h_{em} are the illumination and the emission amplitude distributions. As mentioned above, the illumination is constant along the line, i.e., in the y-direction, and similar to that of point illumination perpendicular to the line, i.e., in the x-direction. Detection-wise, the Airy disk diameter of our setup, i.e., the diameter of the main lobe of the diffraction pattern of the objective lens when utilizing the full NA, amounts to $d = 1.2\lambda/\text{NA} \approx 500$ nm. The pixel size as projected into sample space is 200 nm, and the slit width is adjusted to match the pixel size. Thus, the detection area is much smaller than the diffraction limit and $S(x, y)$ can be approximated as Dirac delta function, especially in the context of FCS where the PSF is subsequently described as a Gaussian function as discussed in detail elsewhere (Hess and Webb 2002). The convolution reduces to multiplication with unity and Eq. 5 simplifies to

$$\begin{aligned}\Psi(x,y,z) &= \text{PSF}_{\text{ill}}(x,z)\cdot\text{PSF}_{\text{det}}(x,y,z)\\ &= |h_{\text{ill}}(x,z)|^2|h_{\text{em}}(x,y,z)|^2\end{aligned} \tag{6}$$

A good approximate yet analytical approach to compute the PSF is based on the scalar Debye theory (Hecht 1989). The amplitude of the electromagnetic field at a point near the focus is expressed as the superposition of plane waves integrated over the lens aperture field. Inserting the properties of the optical system, in particular the NA of the objective lens and the illumination geometry, the combined PSF of the STFM is given as:

$$\Psi(x,y,z) = \left(\frac{\sin(u_{\text{ill}})}{u_{\text{ill}}}\right)^2 \cdot \left(\frac{\sin(u_{\text{det}})}{u_{\text{det}}}\right)^2 \cdot \left(\frac{\sin(v_{x,\text{ill}})}{v_{x,\text{ill}}}\right)^2 \cdot \left(\frac{2J_1(v_{\text{det}})}{v_{\text{det}}}\right)^2 \tag{7}$$

$$u_{\text{ill}} = n\frac{2\pi}{\lambda_{\text{ill}}} z \sin^2(\alpha/2), \quad u_{\text{det}} = n\frac{2\pi}{\lambda_{\text{det}}} z \sin^2(\alpha/2),$$
$$v_{x,\text{ill}} = n\frac{2\pi}{\lambda_{\text{ill}}} x \sin\alpha \quad \text{and} \quad v_{\text{det}} = n\frac{2\pi}{\lambda_{\text{det}}}\sqrt{x^2+y^2}\sin\alpha$$

The effective aperture is slit-like for both axial contributions as well as for the x component of the illumination, resulting in a sin c function distribution. The effective aperture is point-like for the y-component of the illumination and gives a constant contribution. It is circular for the lateral component of the detection, yielding a distribution described with the first-order Bessel function J_1.

Equation 7 makes use of the definition of the propagation wavenumber $k = 2\pi n/\lambda$, the illumination wavelength λ_{ill}, the detection wavelength λ_{det}, the refractive index n, and the aperture angle of the incident light α. General properties of the sin c and Bessel functions are their side lobes that contribute to the intensity profile. As these functions are squared, the first side lobes of the Bessel function reduce to 1.75% and those of the sin c function to 4.7% of the height of the main lobe. The size of the illumination PSF and the detection PSF are different since they scale with different wavelengths. As they are multiplied with each other, the side lobes of the sin c function and those of the Bessel function for the x- and z-direction decrease nearly to zero. However, in the y-direction (along the line) these side lobes cannot be neglected (Dusch et al. 2007). In order to derive an expression for the correlation function in the STFM, we approximate the main lobe and the first side lobes of the PSF as three Gaussian functions. Thus, the resulting correlation function contains not only the contribution from diffusion within the main and the side lobes but also from diffusion between them.

One of the major advantages of a multifocal system is the availability of spatial cross-correlations between different pixels. Based on the expressions given in previous studies for a freely and isotropically diffusing single species (Brinkmeier et al. 1999; LeCaptain and Van Orden 2002) and neglecting correlations between the side lobes, a general expression for the cross-correlation of the fluorescence signal from two pixels k and l of the detection line for the STFM is given as

$$\begin{aligned} G_{kl}(\tau) = {} & \frac{1}{cV_{\text{eff}}}\left(1+\frac{\tau}{\tau_{\text{diff}}}\right)^{-\frac{1}{2}}\left(1+\frac{1}{\kappa_z^2}\frac{\tau}{\tau_{\text{diff}}}\right)^{-\frac{1}{2}} \\ & \times \left\{\frac{1}{1+2A_{1\text{sl}}}\left(1+\frac{1}{\kappa_{y,\text{ml}}^2}\frac{\tau}{\tau_{\text{diff}}}\right)^{-\frac{1}{2}}\right. \\ & \times \exp\left(-\frac{d_{kl}^2}{\kappa_{y,\text{ml}}^2 w_0^2}\left(1+\frac{1}{\kappa_{y,\text{ml}}^2}\frac{\tau}{\tau_{\text{diff}}}\right)^{-1}\right) \\ & + \frac{\kappa_{y,\text{ml}}A_{1\text{sl}}}{\kappa_{y,1\text{sl}}(1+2A_{1\text{sl}})}\left(1+\frac{1}{\kappa_{y,1\text{sl}}^2}\frac{\tau}{\tau_{\text{diff}}}\right)^{-\frac{1}{2}} \\ & \times \left[\exp\left(-\frac{(d_{kl}-y_{1\text{sl}})^2}{\kappa_{y,1\text{sl}}^2 w_0^2}\left(1+\frac{1}{\kappa_{y,1\text{sl}}^2}\frac{\tau}{\tau_{\text{diff}}}\right)^{-1}\right)\right. \\ & \left.\left.+\exp\left(-\frac{(d_{kl}+y_{1\text{sl}})^2}{\kappa_{y,1\text{sl}}^2 w_0^2}\left(1+\frac{1}{\kappa_{y,1\text{sl}}^2}\frac{\tau}{\tau_{\text{diff}}}\right)^{-1}\right)\right]\right\} \end{aligned} \tag{8}$$

with the relative side-lobe amplitude $A_{1\text{sl}}$, the main-lobe-to-side-lobe distance $y_{1\text{sl}}$, and the main- and side-lobe structure parameters $\kappa_{y,1\text{sl}}$, $\kappa_{y,\text{ml}}$ given as

$$A_{1\text{sl}} = 0.0175, \quad y_{1\text{sl}} = \frac{5.14\cdot\lambda_{\text{det}}}{2\pi\cdot n\cdot\sin\alpha},$$
$$\kappa_{y,1\text{sl}} = \frac{w_{y,1\text{sl}}}{w_0} = 0.342\cdot\kappa_{y,\text{ml}}, \quad \kappa_{y,\text{ml}} = \frac{w_{y,\text{ml}}}{w_0} \tag{9}$$

The other parameters are defined in the "Materials and methods" section. The displacement along the line between the two foci is given by the pixel pitch of the EM-CCD camera divided by the total magnification of the system multiplied by their index distance, $d_{kl} = |k-l|\cdot 200$ nm. It is noted that no focal displacement in x or z exists because of the absence of any chromatic shift in a single-color system. Due to the small size of the side-lobe amplitude, the inverted amplitude of the correlation function remains a good approximation for the number of particles in the volume of the main lobe, $V_{\text{eff}} = \pi^{3/2}\kappa_{y,\text{ml}}\kappa_z w_0^3$. However, for a proper analysis of the diffusion process, the side-lobe contribution to the correlation function must be taken into consideration. In the case of anomalous diffusion (Wachsmuth et al. 2000), the different scaling of the mean-squared displacement with time is represented by the

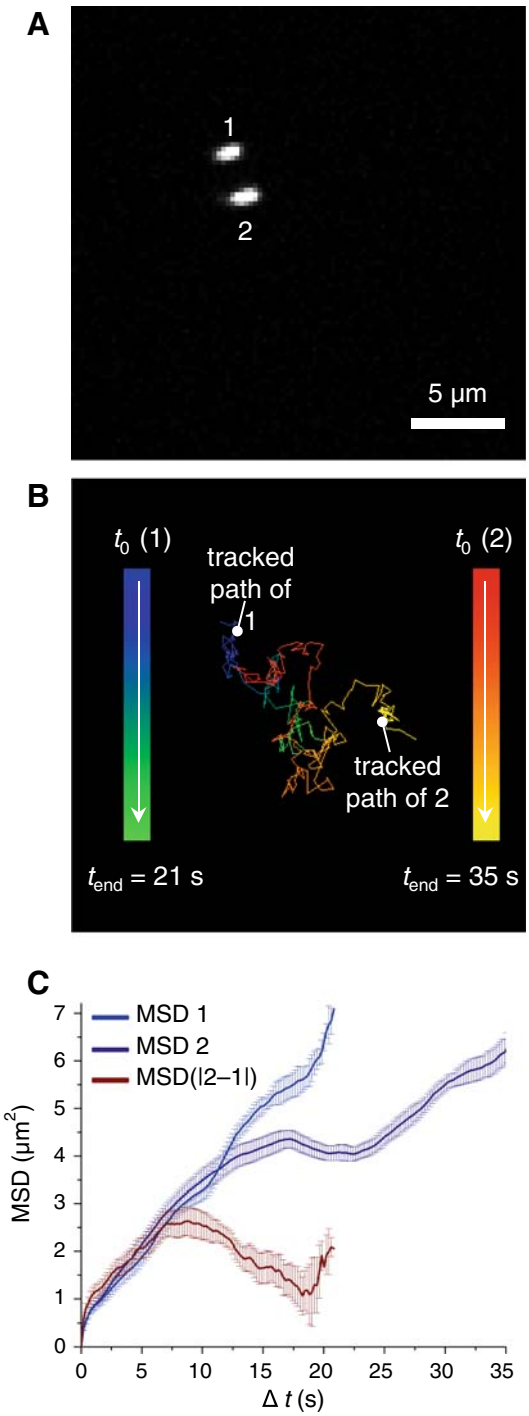

◀ **Fig. 3a–c** Tracking of PML-NBs by fast confocal imaging. **a** STFM image of two fluorescently labeled PML nuclear bodies inside a cell nucleus of a human U2OS osteosarcoma cell. **b** The PML-NBs were tracked in an optical section for 21 and 35 s, respectively, and represented in a color-coded trajectory plot. **c** The mean-squared displacement was calculated for each time Δt with a resolution of 0.2 s (*blue*). The movement of the bodies is also displayed as the change in the distance between bodies 1 and 2 to account for any movements of the cell during the observation period (*red*). The errors were determined from the multiple MSD displacement measured for a certain Δt from the trajectory of a given PML body. These do not represent the "true" mobility variations of PML-NBs since the observation time of 20–30 s was too short to reach the equivalent to measurements of a representative ensemble according to the ergodic principle. This is also apparent from the differences between the two different trajectories shown. For averaged mobility values of PML-NBs, see refs. Görisch et al. (2004) andd Jegou et al. (2009)

anomaly parameter α and by replacing τ/τ_{diff} with $(\tau/\tau_{diff})^{\alpha}$, resulting in a modified correlation function.

Single-particle tracking of PML nuclear-body movements with the STFM

PML nuclear bodies are mobile subcompartments in the nucleus that have been shown to be involved in different processes such as apoptosis, senescence, cell proliferation, chromatin remodeling, DNA damage repair, transcription, and telomere lengthening (Görisch et al. 2005; Görisch et al. 2004; Jegou et al. 2009; Lamond and Sleeman 2003). PML-NBs have typical diameters of 0.2–1 µm and are formed by PML and Sp100 proteins. Via labeling with GFP-PML III, their mobility can be studied in single-particle tracking experiments. Due to the time resolution of conventional CLSM, information about their mobility has been limited to a time scale well above 1 s (Görisch et al. 2004). Here, the fast-imaging feature of the STFM was applied to study their translocation below this time regime. Figure 3 displays representative mobility measurements of two fluorescently labeled nuclear bodies. Each nuclear body was tracked over time as displayed in the color-coded trajectory (Fig. 3b). The mean-squared displacement (MSD) was calculated for each PML body (Fig. 3c). Comparing the MSD curves (blue) with the ΔMSD curve for PML nuclear bodies 1 and 2 (red), it is apparent that each body moved quickly through the nucleus resulting in a large MSD value. However, the distance between them is more or less constant as represented by relatively low ΔMSD values. An additional advantage of these ΔMSD curves is the elimination of the translational movements of the whole cell nucleus, which is essential for MSD measurements of PML-NBs on the minute time scale (Jegou et al. 2009).

STFM time traces of 100-nm beads along a line

The concept of multifocal FCS experiments along a line with the STFM can be directly visualized by measurements with fluorescently labeled 100-nm polystyrene nanospheres. A 128-pixel line of the detector was read out at a rate of 380 lps for a total of 13 s as displayed as the fluorescence intensity along the detected line (*y*-axis)

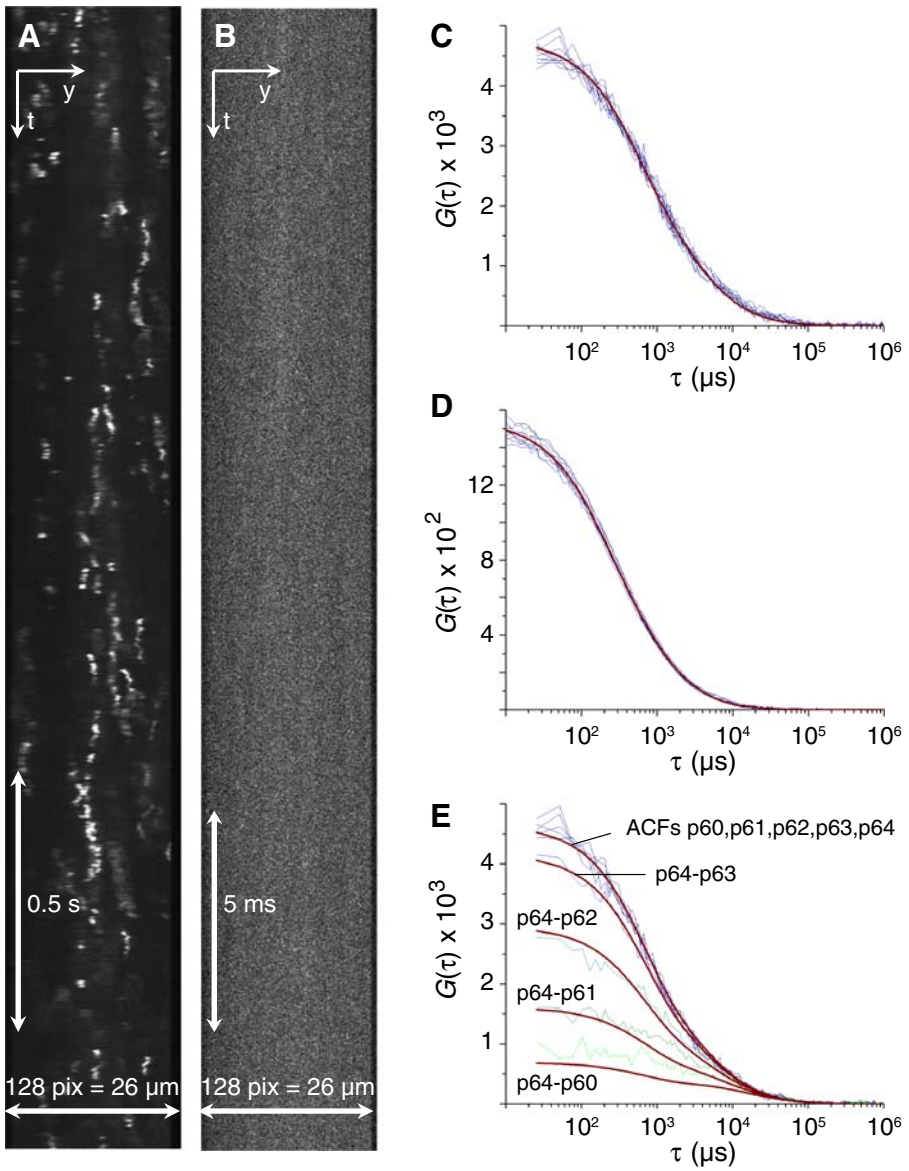

Fig. 4a–e Mobility analysis of fluorescently labeled 100-nm beads and quantum dots. **a** Position-time images of fluorescently labeled 100-nm beads floating freely through the line-shaped focal volume are shown. In the image, the position along the detector array is plotted horizontally. The vertical time axis was acquired with a resolution of 380 lps. **b** STFM time-trace image of green-fluorescent quantum dot Qdot525 streptavidin conjugates. The vertical time axis was acquired with 38,900 lps. **c** STFM autocorrelation function from quantum dots determined at 10 different positions from pixel 55 to pixel 64. The *solid dark red line* is a fit to the autocorrelation data yielding a concentration of $c = 200 \pm 10$ nM, $\tau_{diff} = 1{,}600 \pm 50$ µs, and $D = 14.1 \pm 0.1$ µm^2·s^{-1} with a fixed lateral focus radius of $\omega_0 = 300$ nm as determined from the cross-correlation curves (see below). Diffusion coefficients were calculated from the measured diffusion times according to $D = \omega_0^2/4\tau_{diff}$. **d** Autocorrelation functions from 10 measurements with point FCS and fit (*solid dark red line*) with $c = 49 \pm 3$ nM, $\tau_{diff} = 490 \pm 12$ µs, $\omega_0 = 170 \pm 10$ nm (determined with an Alexa 488 reference solution), and $D = 14.7 \pm 0.5$ µm^2 s^{-1}. **e** STFM spatial cross-correlation curves of a quantum dot sample determined for neighboring pixels along the detector array between pixels 60 and 64, 61 and 64, 62 and 64, as well as 63 and 64. For comparison, the autocorrelation functions (ACFs) of the five pixels 60 to 64 are shown too. It can be seen that for the cross-correlation curves, the amplitude decreases with increasing pixel distances as expected. From a fit of cross-correlation curves (*solid dark red line*), the lateral focus radius of $\omega_0 = 300 \pm 10$ nm (as a global fit parameter in all four curves) was determined for the STFM instrument

versus time (Fig. 4a). This sampling speed is sufficient to resolve the relatively slow-moving beads. The experiment revealed and visualized the fluctuations of the fluorescence intensity due to random particle movements. When the fluorescently labeled beads enter the illumination volume, they give rise to fluorescence signal at the entry point on the line detector. Diffusion along the line can then be monitored by position fluctuations that appear as diagonal

translocations in the time trace. The beads disappear as they leave the illumination volume perpendicular to the line in the x- or z-direction, so that the vertical length of each trajectory yields the corresponding dwell time in the illumination volume. This was typically below 0.5 s. Horizontally, the trajectories never spanned more than 25 pixels corresponding to 5 μm in the experiments. This measurement illustrates the principle of line FCS measurements with the STFM.

In vitro FCS analysis of the mobility of quantum dots with the STFM

For faster movements of smaller particles, the intensity fluctuations due to movements in and out of the detection volume can no longer be resolved by simple time-trace imaging. This was demonstrated by imaging quantum dots (Qdot525 streptavidin conjugates with a particle size of ~15 nm) with the STFM at a acquisition rate of 38,900 lps (Fig. 4b). The diffusion time of these particles could only be determined by calculating the STFM autocorrelation function from the intensity fluctuations according to Eq. 8. This is shown for 10 positions from pixel 55 to pixel 64 along the detector array in Fig. 4c, for which the measured diffusion times corresponded to $D = 14.1 \pm 0.1$ μm^2 s^{-1}. To evaluate the performance of the STFM instrument, 10 conventional FCS autocorrelation curves were acquired from successive point measurements for the same sample (Fig. 4d). The autocorrelation function $G(\tau)$ was fitted to Eq. 4. From this analysis, $D = 14.7 \pm 0.5$ μm^2 s^{-1} was retrieved. Thus, the mobility determination with the STFM was in excellent agreement with the conventional point FCS measurements. For the fit of the STFM autocorrelation function, the size of the STFM lateral focus radius was determined to be $\omega_0 = 300 \pm 10$ nm from the spatial cross-correlation curves of neighboring pixels along the detector array of the STFM (Fig. 4e). Particle movements of more than 200 nm (=1 pixel size) apart were assumed to be independent, which implies that the cross-correlations of the intensity signals detected at two neighboring pixels originate only from the cross-talk between them and not from correlated movements of the particles in these foci. Cross-correlation functions between the intensity signals of several consecutive pixels along the detection line depend largely on the size of the focus, so that $\omega_0 = 300 \pm 10$ nm could be determined from the fit of this parameter (Eq. 8). This is a straightforward approach to determine the lateral focus radius that is not available for the point FCS instrument. For the latter, $\omega_0 = 170 \pm 10$ nm was determined with an Alexa Fluor 488 maleimide reference solution according to its previously determined diffusion coefficient of $(2.1 \pm 0.21) \times 10^{-6}$ cm^2 s^{-1}.

Intracellular mobility of GFP measured by FCS with the STFM

FCS is a well-suited method for the analysis of fast dynamics of proteins fused with the green fluorescent protein (GFP). GFP is a relatively small 27 kDa protein that does not interact with cellular structures. When expressed alone, it is uniformly distributed throughout the cytoplasm and the nucleus without any apparent interactions with nuclear structures and only few areas of reduced concentration due to exclusion from high-density areas such as the nucleolus. To demonstrate the capabilities of the STFM for characterizing the dynamics of cellular processes simultaneously at a series of positions along a line, the instrument was used to acquire concentration fluctuations of GFP in living cells (Fig. 5a–d). The intensity profiles along the indicated line and the corresponding profile of the apparent diffusion coefficients are displayed in Fig. 5b and c. The profiles of the diffusion coefficients were derived from the diffusion times, τ_{diff}, determined from the autocorrelations of the measured intensity profile over a period of 90 s for each pixel along the line. A spatially resolved GFP mobility with diffusion coefficients ranging from 15 to 27 μm^2 s^{-1} was obtained (Fig. 5c). Four exemplary autocorrelation functions corresponding to the four indicated positions in Fig. 5a along the lines are displayed in Fig. 5d. These experiments were compared to conventional single-point FCS measurements with the same batch of GFP-expressing HeLa cells (Fig. 5e). In these experiments, similar variations of the diffusion coefficient were measured in different cellular locations in the cytoplasm and the nucleus with values ranging from 16–26 μm^2 s^{-1}. However, it is noted that the sequential data acquisition in the point FCS experiments precludes a clear distinction between true spatial variations in the GFP mobility as opposed to variations that reflect changes in the cell state. In contrast, it is clear from the STFM analysis that local variations in GFP mobility exist in the cell.

Dynamics of the chromatin-remodeling complex Snf2H measured by STFM

In the cell nucleus, the DNA is compacted by histone proteins into a nucleoprotein complex termed chromatin (van Holde 1989). The central building block of chromatin is the cylindrically shaped nucleosome (11 nm diameter, 5.5 nm height). It comprises an octamer core of two copies each of histones H2A, H2B, H3, and H4 around which the DNA is wrapped in 1.67 turns. Chromatin remodelers are molecular machines that can translocate nucleosomes along the DNA sequence upon hydrolysis of ATP, making the corresponding sites accessible for the binding of other

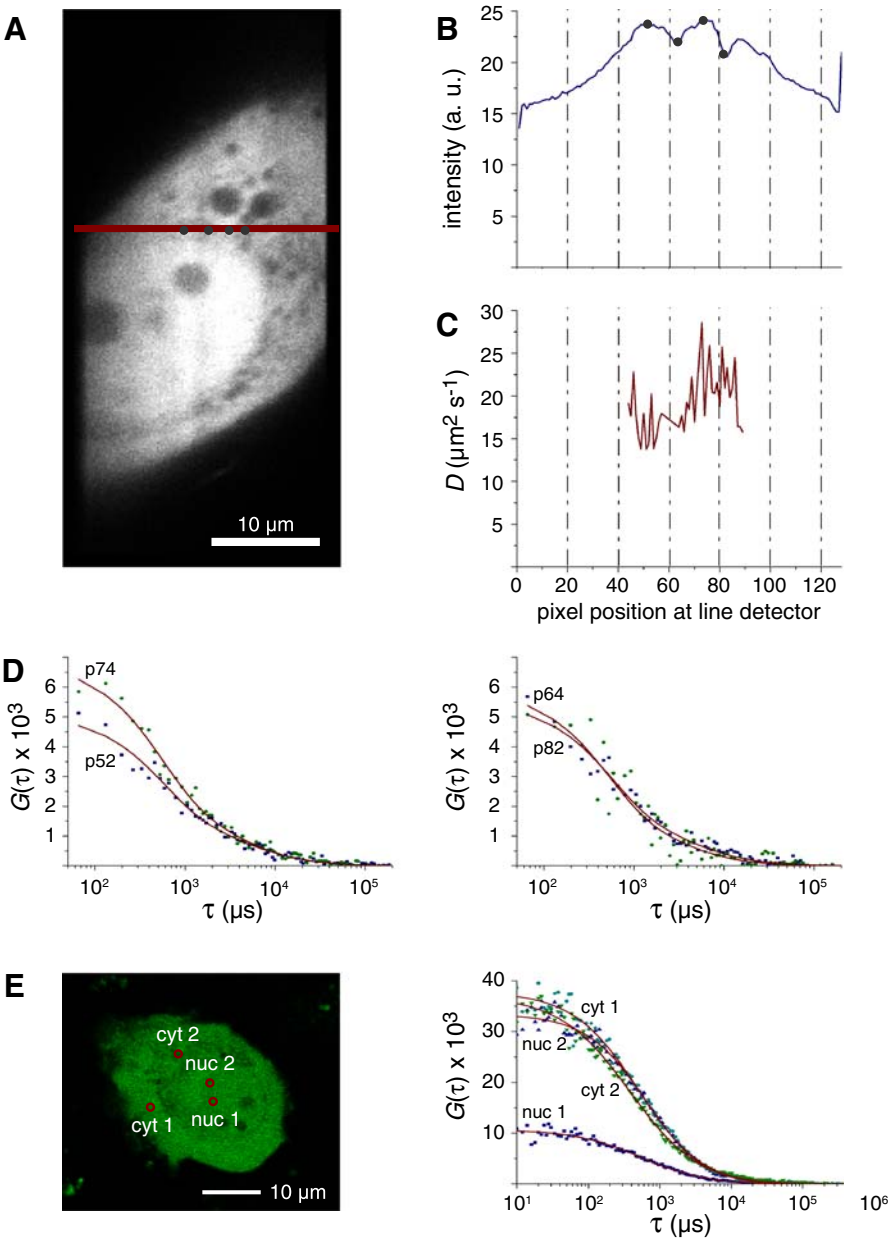

Fig. 5a–e STFM measurement of GFP in living HeLa cells. **a** STFM fluorescence image of a cell transfected with GFP. Pixels 52, 64, 74, and 82 on the line are indicated. **b** Fluorescence intensity distribution measured with the STFM along the indicated line. **c** Distribution of corresponding diffusion coefficients along the line. These were determined by autocorrelation of each pixel intensity over time. **d** STFM autocorrelation curves and fits for the four different pixels indicated in **a**. Pixel 52, $\tau_{diff} = 1.64 \pm 0.30$ ms, $c = 180 \pm 10$ nM; pixel 74, $\tau_{diff} = 1.25 \pm 0.21$ ms, $c = 140 \pm 10$ nM; pixel 64, $\tau_{diff} = 1.42 \pm 0.25$ ms, 170 ± 10 nM; pixel 82, τ_{diff} 0.98 ± 0.16 ms, $c = 160 \pm 10$ nM. **e** Conventional point FCS of GFP mobility in the same cells. The *left panel* shows the CLSM image with the *red circles* indicating the four different positions of FCS measurements in the cytoplasm and the nucleus. The *right panel* shows autocorrelation curves and their corresponding fit functions in the cytoplasm with $c_{cyt,1} = 130 \pm 10$ nM, $D_{cyt,1} = 19.9 \pm 0.5$ µm^2 s^{-1}, $\alpha_{cyt,1} = 0.95 \pm 0.02$, $c_{cyt,2} = 130 \pm 10$ nM, $D_{cyt,2} = 25.8 \pm 0.9$ µm^2 s^{-1}, and $\alpha_{cyt,2} = 0.88 \pm 0.02$. Fit parameters in the nucleus were $c_{nuc,1} = 460 \pm 30$ nM, $D_{nuc,1} = 18.4 \pm 1.7$ µm^2 s^{-1}, $\alpha_{nuc,1} = 0.93 \pm 0.06$, $c_{nuc,2} = 150 \pm 10$ nM, $D_{nuc,2} = 15.6 \pm 0.4$ µm^2 s^{-1}, and $\alpha_{nuc,2} = 1.04 \pm 0.02$

factors (Becker and Horz 2002; Cairns 2007; Längst and Becker 2001; Rippe et al. 2007). Here, the intracellular mobility of one class of chromatin-remodeling complexes that uses the ATPase subunit Snf2H (Collins et al. 2002; Längst and Becker 2001; Rippe et al. 2007) was investigated. FCS experiments with the STFM were conducted in U2OS cells stably expressing Snf2H-GFP (Fig. 6). The autocorrelation function for every pixel was calculated and

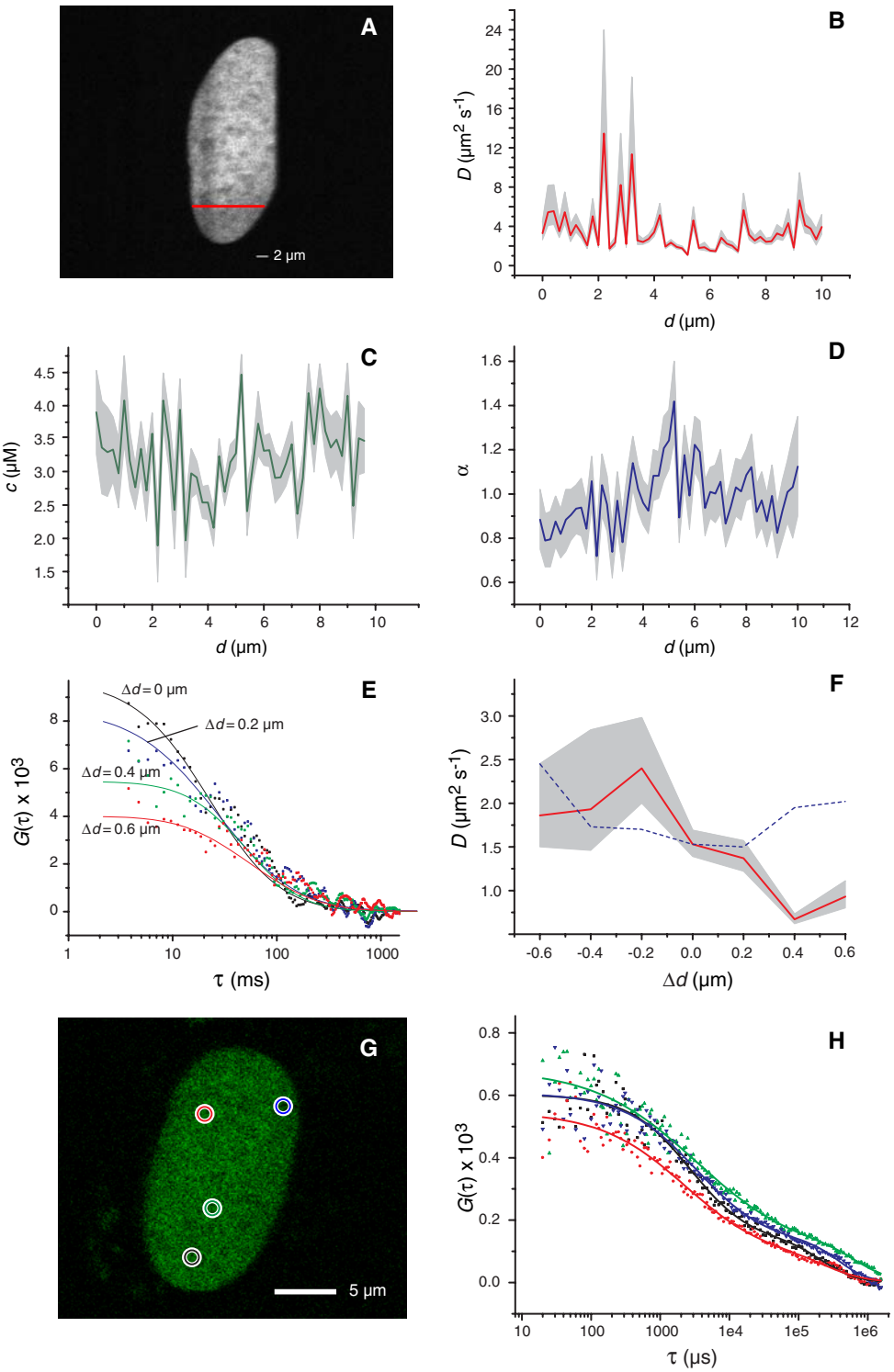

Fig. 6a–h STFM auto/cross-correlation analysis of Snf2H-containing chromatin-remodeling complexes in U2OS cells. **a** Nucleus of a U2OS cell stably transfected with Snf2H-GFP. The illuminated line is shown in *red*. Spatially resolved values for the apparent diffusion coefficient (**b**), concentration (**c**), and anomaly parameter (**d**) were calculated. Values are plotted with 95% confidence intervals (*gray*). **e** Spatial cross-correlation functions and fits for the pixel distances 0.2, 0.4, and 0.6 µm (to the right of the pixel at 6 µm). **f** Apparent diffusion coefficients obtained by fitting the spatial cross-correlation function calculated between the pixel at 6 µm and different pixels at distance Δ (*red line*, 95% confidence intervals shown in *gray*). **g** CLSM image of Snf2H-GFP nuclear distribution with indicated locations of conventional point FCS of Snf2H-GFP. **h** Autocorrelation functions and their corresponding fit function from the point FCS system at the positions indicated in **g**. Since Snf2H interacts with chromatin, two species were present in the autocorrelation functions. The apparent diffusion coefficients for the fast species as well as the concentrations of the mobile Snf2H-GFP were derived as $D_1 = 2.5 \pm 0.5$ µm^2 s^{-1}, $c_1 = 1.5 \pm 0.1$ µM (*green line*); $D_2 = 2.4 \pm 0.3$ µm^2 s^{-1}, $c_2 = 1.7 \pm 0.1$ µM (*blue line*); $D_3 = 2.9 \pm 0.4$ µm^2 s^{-1}, $c_3 = 1.7 \pm 0.1$ µM (*black line*); $D_4 = 3.4 \pm 0.4$ µm^2 s^{-1}, $c_4 = 1.9 \pm 0.1$ µM (*red line*)

fitted to the expression for anomalous diffusion, resulting in spatially resolved profiles for the apparent diffusion coefficient, the concentration (of the mobile protein pool), and the anomaly parameter. As average values for the FCS line measurements with the STFM an apparent diffusion coefficient $D_{app} = 3.5 \pm 0.6$ (± 0.4) µm^2 s^{-1}, a concentration $c = 3.2 \pm 0.1$ (± 0.4) µM, and an anomaly parameter $\alpha = 0.98 \pm 0.02$ (± 0.13) were determined. Values are reported with standard deviation and typical 95% confidence interval in brackets. The average values were similar to the results obtained with point FCS measurements (Fig. 6g, h). For the anomaly parameter, the

standard deviation was smaller than the typical 95% confidence interval, indicating that this parameter is rather uniform in the cell. However, for the apparent diffusion coefficient, the standard deviation is larger than the typical 95% confidence interval, suggesting that Snf2H mobility is not homogeneous throughout the cell. Indeed, it can be seen from inspection of Fig. 6b that at the pixel positions $d = 2$ to 4 μm, regions of locally increased Snf2H-GFP mobility exist. An alternative analysis method for STFM data is the calculation of the spatial cross-correlation function between different pixels. Compared to the autocorrelation analysis, this approach benefits from the fact that a well-defined distance, i.e., the distance between the two correlated pixels, is used to calculate the diffusion coefficient. In the case of an autocorrelation analysis, the focus radius—which cannot be determined as precisely as the pixel distance—is used instead. The spatial cross-correlation functions for the pixel at $d = 6$ μm with three neighboring pixels on each side were calculated and fitted according to Eq. 8. The results confirmed the mobility measured in the autocorrelation analysis (Fig. 6e, f).

Discussion

To advance the spatially resolved analysis of macromolecule dynamics in living cells, the existing CLSM-based approach with point illumination/detection was extended here to a new scanning microscope with a line illumination and confocal line detection system. This instrument, the STFM, enables the detection of fluorescence intensity fluctuations due to concentration fluctuations of randomly diffusing particles simultaneously at a series of foci along a line, providing a one-dimensional map of the respective diffusion properties. Although the resolution of the STFM of 200 × 380 × 700 nm in x-, y-, and z-directions is not quite as good as that of a point CLSM, the STFM has a number of advantages. For the current setup, the acquisition rate can be as fast as 70,000 lines per second (for a line of 128 pixels), corresponding to one-dimensional measurements with 14 μs time resolution or 30 images per second (33 ms time resolution) for an image size of 25 × 25 μm (128 × 128 pixels). This allows for live-cell imaging experiments, single-particle tracking, and fluctuation microscopy techniques. While the imaging speed as measured in frames per second is comparable to that of fast point CLSMs, the STFM outperforms existing multifocal or scanning fluorescence fluctuation spectroscopy approaches. Since pixels along the line are imaged simultaneously with good lateral and axial resolution, information on particle dynamics as extracted with correlation analyses is obtained that is available neither from conventional CLSM imaging (typically suffering from insufficient temporal sampling for every pixel) nor from conventional point FCS (which does not provide any spatially differentiated information).

In the present study, the concept and the implementation of the STFM as well as theoretical considerations for particle tracking and FCS data as acquired with the STFM were presented. Using appropriate approximations, we have derived a description for the PSF of a line-scanning confocal setup such as the STFM that is in agreement with previous results (Dusch et al. 2007). We have used this to obtain an analytical expression for the temporal autocorrelation and the spatial cross-correlation function in such a setup. A comparison of STFM measurements with conventional point FCS experiments using quantum dots demonstrated the validity of our theoretical framework. It can be easily extended to more complex polydisperse systems as well as to anomalous diffusion processes or the use of two (or more) excitation and detection channels.

While the maximum imaging speed of the STFM is comparable to fast CLSMs, the parallelized acquisition results in an illumination and integration time that is two to three orders of magnitude longer so that the illumination intensity can be reduced. This has several advantages: the very high illumination intensity usually required to obtain a high frame rate with a resonant scanner CLSM often results in saturation and an increased effective size of the PSF, i.e., the resolution deteriorates and approaches that of the STFM. In addition, high illumination intensities often generate a large population of fluorophores in triplet states or undergoing photobleaching, thus reducing the overall yield of photons from a sample.

Several exemplary applications of the STFM are reported that include the determination of the mobility of nanobeads and quantum dots in solution as well as the tracking of PML nuclear bodies and FCS measurements of GFP and the chromatin-remodeling factor Snf2H in living cells. The analysis of PML-NBs, GFP, and Snf2H gave new insight into their dynamics. In previous studies, we have reported on the multiscale mobility of PML-NBs that reflects features of the chromatin environment (Görisch et al. 2004; Jegou et al. 2009; Wachsmuth et al. 2008). On the minute time scale, the movement can be described by a diffusion-like motion of the PML-NB's center of mass in a corral with a radius of 200–300 nm that can further translocate due to the movement of larger chromatin domains. The STFM tracking experiments of PML-NBs conducted here with a 0.2 ms time resolution revealed that significant movements on the scale of several hundreds of nanometers occur already on the second time scale. It is noted that the apparent mobility of nuclear bodies as described by their MSD/diffusion coefficient and accessible space is highly dependent on the observation period, as both parameters are affected by the different levels of

chromatin organization (Wachsmuth et al. 2008). Thus, it is essential to combine tracking experiments conducted on different time scales for a complete description of particle mobility as demonstrated recently in the context of telomere mobility (Jegou et al. 2009).

For the analysis of fluorescent particle mobilities that are not accessible to SPT approaches, the existing implementation of a point FCS method was extended in the STFM to FCS measurements along a line. This was applied first to acquiring fluctuations of the green fluorescent protein (GFP) in living cells. GFP is a relatively small protein and is uniformly distributed throughout the nucleus without any apparent interactions with nuclear structures. Previous FCS experiments on monomeric GFP in living cells showed that diffusion of GFP was essentially independent of its cellular localization, e.g., measurements of GFP in the nucleus and in the cytoplasm yielded indistinguishable results (Beaudouin et al. 2006; Berland et al. 1995; Pack et al. 2006; Wachsmuth et al. 2000). In these studies an averaged diffusion coefficient of $D = 23\ \mu m^2\ s^{-1}$ was measured in the cell that reflected an apparent 3.5-fold higher viscosity of the cellular environment as compared to water (Wachsmuth et al. 2008). While FCS point measurements in previous studies displayed some variability (see also Fig. 4e), no spatially dependent mobility of GFP was apparent after averaging successive measurements. In the STFM analysis, the averaged GFP diffusion coefficient was $20\ \mu m^2\ s^{-1}$ and similar to both the previously reported value and to that of the point FCS analysis of the same cells with diffusion coefficients of 16–26 $\mu m^2\ s^{-1}$. However, the diffusion coefficient appeared to be reduced by about 20% in the nucleus as compared to the cytoplasm (Fig. 5). Thus, we conclude that even for a small inert particle such as GFP, significant variations exist at different locations in the cell that can be resolved with the STFM.

In terms of biological functions, another important aspect of intracellular translocations is the binding to cellular structures. In particular, numerous chromatin interacting proteins display binding and dissociation to and from chromatin with residence times in the bound state that are characteristic for their specific genome activity (Wachsmuth et al. 2008). Here, we have characterized the spatial profile of the apparent diffusion coefficient for the Snf2H chromatin remodeler. Although chromatin-remodeling complexes have been shown in several studies to possess distinct nucleosome/DNA binding and remodeling capabilities in vitro (e. g., Becker and Horz 2002; Cairns 2007; Längst and Becker 2001; Rippe et al. 2007 and references therein), little is known on how they operate in the cell. In a previous study, Varga-Weisz and colleagues used conventional confocal fluorescence microscopy to study Snf2H and its associated Acf1 subunit (Collins et al. 2002). Their work revealed the overall Snf2H/Acf1 nuclear distribution with an enrichment in pericentric heterochromatin foci of mouse cells that have typical diameters of $\sim 1\ \mu m$. These nuclear substructures are not present on fluorescence microscopy images of the chromatin in human cells as in the U2OS line studied here. Accordingly, the nuclear distribution of Snf2H in these cells appears more homogeneous on the images than in the mouse fibroblasts used by Varga-Weisz and colleagues. Nevertheless, the STFM experiments conducted with Snf2H reveal variations in the apparent diffusion coefficient indicating that the interaction behavior of Snf2H and its complexes is rather heterogeneous. The spatial profile of the apparent diffusion coefficient shows that Snf2H is freely mobile at only a few sites in the cell (see region between 2 and 4 μm in Fig. 6b). From FCS measurements of Snf2H in the cytoplasm, it can be inferred that the free diffusive mobility of Snf2H in the environment of the cell corresponds to $D = 13 \pm 1\ \mu m^2\ s^{-1}$. Thus, Snf2H is slowed down significantly due to binding interactions within the nucleus. The mobility profile spans 10 μm through the nucleus and thus covers euchromatin as well as heterochromatin. This suggests that Snf2H or its complexes undergo binding to both chromatin states, which is confirmed by point FCS measurements in mouse cells (data not shown). Moreover, distinct regions appear to be present that show a value of $D \sim 10\ \mu m^2\ s^{-1}$. Accordingly, nuclear regions exist in which the Snf2H remodeler is almost freely mobile and displays very little interaction with chromatin. This is in agreement with a recent high-resolution study on the nuclear distribution of Snf2H with respect to nucleosomes in U2OS cells by dual-color localization microscopy (Gunkel et al. 2009).

In summary, the STFM instrument introduced here allows for quantitative and spatially resolved measurements of the mobility of molecules as well as larger subcellular structures on various time scales with diffraction-limited spatial resolution. It is anticipated that its unique capabilities will prove to be a highly valuable addition to the currently available repertoire of methods for studying the dynamics and interactions of proteins in living cells.

Acknowledgments We are indebted to Christoph Cremer for his continuous support of the development of the STFM instrument at the Kirchhoff-Institut für Physik, and thank Felix Bestvater, Zahir Seghiri, Moon Sik Kang, Katharina Müller, and Michael Tewes for help and discussions as well as Werner Knebel from Leica Microsystems and Peter Vogt from Coherent for technical support. The detailed comments and suggestions of one of the reviewers for the revision of the paper are gratefully acknowledged. The work was funded by the Volkswagenstiftung and by the Deutsche Forschungsgemeinschaft within the Research Training Group "Molecular imaging methods for the analysis of gene and protein expression" (GRK 886/1) and by grants Ri 1283/5-3 (SPP1128 priority program "Optical analysis of structure and dynamics of supramolecular biological complexes") and Ri 1283/8-1.

References

Axelrod D, Koppel DE, Schlessinger J, Elson E, Webb WW (1976) Mobility measurement by analysis of fluorescence photobleaching recovery kinetics. Biophys J 16:1055–1069

Bayer J, Radler JO (2006) DNA microelectrophoresis using double focus fluorescence correlation spectroscopy. Electrophoresis 27:3952–3963

Beaudouin J, Mora-Bermúdez F, Klee T, Daigle N, Ellenberg J (2006) Dissecting the contribution of diffusion and interactions to the mobility of nuclear proteins. Biophys J 90:1878–1894

Becker PB, Horz W (2002) ATP-dependent nucleosome remodeling. Annu Rev Biochem 71:247–273

Berland KM, So PT, Gratton E (1995) Two-photon fluorescence correlation spectroscopy: method and application to the intracellular environment. Biophys J 68:694–701

Berland KM, So PTC, Chen Y, Mantulin WW, Gratton E (1996) Scanning 2-photon fluctuation correlation spectroscopy—particle counting measurements for detection of molecular aggregation. Biophys J 71:410–420

Borlinghaus RT (2006) High speed scanning has the potential to increase fluorescence yield and to reduce photobleaching. Micr Res Tech 69:689–692

Brinkmeier M, Dorre K, Riebeseel K, Rigler R (1997) Confocal spectroscopy in microstructures. Biophys Chem 66:229–239

Brinkmeier M, Dorre K, Stephan J, Eigen M (1999) Two beam cross correlation: a method to characterize transport phenomena in micrometer-sized structures. Anal Chem 71:609–616

Brown CM, Dalal RB, Hebert B, Digman MA, Horwitz AR, Gratton E (2008) Raster image correlation spectroscopy (RICS) for measuring fast protein dynamics and concentrations with a commercial laser scanning confocal microscope. J Microsc 229:78–91

Burkhardt M, Schwille P (2006) Electron multiplying CCD based detection for spatially resolved fluorescence correlation spectroscopy. Opt Exp 14:5013–5020

Cairns BR (2007) Chromatin remodeling: insights and intrigue from single-molecule studies. Nat Struct Mol Biol 14:989–996

Cole NB, Smith CL, Sciaky N, Terasaki M, Edidin M, Lippincott-Schwartz J (1996) Diffusional mobility of Golgi proteins in membranes of living cells. Science 273:797–801

Collins N, Poot RA, Kukimoto I, Garcia-Jimenez C, Dellaire G, Varga-Weisz PD (2002) An ACF1-ISWI chromatin-remodeling complex is required for DNA replication through heterochromatin. Nat Genet 32:627–632

Cutts LS, Roberts PA, Adler J, Davies MC, Melia CD (1995) Determination of localized diffusion coefficients in gels using confocal scanning laser microscopy. J Microsc 180:131–139

Digman MA, Brown CM, Sengupta P, Wiseman PW, Horwitz AR, Gratton E (2005a) Measuring fast dynamics in solutions and cells with a laser scanning microscope. Biophys J 89:1317–1327

Digman MA, Sengupta P, Wiseman PW, Brown CM, Horwitz AR, Gratton E (2005b) Fluctuation correlation spectroscopy with a laser-scanning microscope: exploiting the hidden time structure. Biophys J 88:L33–L36

Dusch E, Dorval T, Vincent N, Wachsmuth M, Genovesio A (2007) Three-dimensional point spread function model for line-scanning confocal microscope with high-aperture objective. J Microsc 228:132–138

Elson EL, Magde D (1974) Fluorescence correlation spectroscopy. I: Conceptual basis and theory. Biopolymers 13:1–27

Gomez DE, Califano M, Mulvaney P (2006) Optical properties of single semiconductor nanocrystals. Phys Chem Chem Phys 8:4989–5011

Görisch SM, Wachsmuth M, Ittrich C, Bacher CP, Rippe K, Lichter P (2004) Nuclear body movement is determined by chromatin accessibility and dynamics. Proc Natl Acad Sci USA 101: 13221–13226

Görisch SM, Lichter P, Rippe K (2005) Mobility of multi-subunit complexes in the nucleus: chromatin dynamics and accessibility of nuclear subcompartments. Histochem Cell Biol 123:217–228

Gunkel M, Erdel F, Rippe K, Lemmer P, Kaufmann R, Hörmann C, Amberger R, Cremer C (2009) Dual color localization microscopy of cellular nanostructures. Biotechnol J (in press)

Hecht E (1989) Optics. Addisson-Wesley, Longmann, New York

Hess ST, Webb WW (2002) Focal volume optics and experimental artifacts in confocal fluorescence correlation spectroscopy. Biophys J 83:2300–2317

Heuff RF, Swift JL, Cramb DT (2007) Fluorescence correlation spectroscopy using quantum dots: advances, challenges and opportunities. Phys Chem Chem Phys 9:1870–1880

Heuvelman G (2008) Development and design of a spatially and temporally resolved fluorescence fluctuation microscope for the analysis of molecular mobilities and interactions. PhD Thesis, Ruprecht-Karls-Universität Heidelberg, Heidelberg

Hwang LC, Wohland T (2007) Recent advances in fluorescence cross-correlation spectroscopy. Cell Biochem Biophys 49:1–13

Jegou T, Chung I, Heuvelmann G, Wachsmuth M, Görisch SM, Greulich-Bode K, Boukamp P, Lichter P, Rippe K (2009) Dynamics of telomeres and promyelocytic leukemia nuclear bodies in a telomerase negative human cell line. Mol Biol Cell 20:2070–2082

Kannan B, Guo L, Sudhaharan T, Ahmed S, Maruyama I, Wohland T (2007) Spatially resolved total internal reflection fluorescence correlation microscopy using an electron multiplying charge-coupled device camera. Anal Chem 79:4463–4470

Kolin DL, Wiseman PW (2007) Advances in image correlation spectroscopy: measuring number densities, aggregation states, and dynamics of fluorescently labeled macromolecules in cells. Cell Biochem Biophys 49:141–164

Kudryavtsev V, Felekyan S, Wozniak AK, Konig M, Sandhagen C, Kuhnemuth R, Seidel CA, Oesterhelt F (2007) Monitoring dynamic systems with multiparameter fluorescence imaging. Anal Bioanal Chem 387:71–82

Lamond AI, Sleeman JE (2003) Nuclear substructure and dynamics. Curr Biol 13:R825–R828

Längst G, Becker PB (2001) Nucleosome mobilization and positioning by ISWI-containing chromatin-remodeling factors. J Cell Sci 114:2561–2568

LeCaptain DJ, Van Orden A (2002) Two-beam fluorescence cross-correlation spectroscopy in an electrophoretic mobility shift assay. Anal Chem 74:1171–1176

Lumma D, Best A, Gansen A, Feuillebois F, Radler JO, Vinogradova OI (2003) Flow profile near a wall measured by double-focus fluorescence cross-correlation. Phys Rev E Stat Nonlin Soft Matter Phys 67:056313

Magde D, Elson EL, Webb WW (1972) Thermodynamic fluctuations in a reacting system—measurement by fluorescence correlation spectroscopy. Phys Rev Lett 29:705–708

Magde D, Elson EL, Webb WW (1974) Fluorescence correlation spectroscopy. II: An experimental realization. Biopolymers 13:29–61

Pack C, Saito K, Tamura M, Kinjo M (2006) Microenvironment and effect of energy depletion in the nucleus analyzed by mobility of multiple oligomeric EGFPs. Biophys J 91:3921–3936

Palmer AG, Thompson NL (1987) Theory of sample translation in fluorescence correlation spectroscopy. Biophys J 51:339–343

Pan X, Foo W, Lim W, Fok MH, Liu P, Yu H, Maruyama I, Wohland T (2007) Multifunctional fluorescence correlation microscope for intracellular and microfluidic measurements. Rev Sci Instrum 78:053711

Pawley JB (ed) (1995) Handbook of biological confocal microscopy, 2nd ed. Plenum, New York

Peters R, Peters J, Tews KH, Bahr W (1974) A microfluorimetric study of translational diffusion in erythrocyte membranes. Biochim Biophys Acta 367:282–294

Peters R, Brünger A, Schulten K (1981) Continuous fluorescence microphotolysis: a sensitive method for study of diffusion processes in single cells. Proc Natl Acad Sci USA 78:962–966

Petrasek Z, Schwille P (2008) Precise measurement of diffusion coefficients using scanning fluorescence correlation spectroscopy. Biophys J 94:1437–1448

Qian H, Elson EL (1991) Analysis of confocal laser-microscope optics for 3-D fluorescence correlation spectroscopy. Appl Opt 30:1185–1195

Rippe K, Schrader A, Riede P, Strohner R, Lehmann E, Langst G (2007) DNA sequence- and conformation-directed positioning of nucleosomes by chromatin-remodeling complexes. Proc Natl Acad Sci USA 104:15635–15640

Ruan Q, Cheng MA, Levi M, Gratton E, Mantulin WW (2004) Spatial-temporal studies of membrane dynamics: scanning fluorescence correlation spectroscopy (SFCS). Biophys J 87: 1260–1267

Schwille P (2003) TIR-FCS: staying on the surface can sometimes be better. Biophys J 85:2783–2784

Sisan DR, Arevalo R, Graves C, McAllister R, Urbach JS (2006) Spatially resolved fluorescence correlation spectroscopy using a spinning disk confocal microscope. Biophys J 91:4241–4252

Skinner JP, Chen Y, Muller JD (2005) Position-sensitive scanning fluorescence correlation spectroscopy. Biophys J 89:1288–1301

van Holde KE (1989) Chromatin. Springer, Heidelberg

Wachsmuth M, Weisshart K (2007) Fluorescence photobleaching and fluorescence correlation spectroscopy: two complementary technologies to study molecular dynamics in living cells. In: Shorte SL, Frischknecht F (eds) Imaging cellular and molecular biological functions. Springer, Heidelberg

Wachsmuth M, Waldeck W, Langowski J (2000) Anomalous diffusion of fluorescent probes inside living cell nuclei investigated by spatially-resolved fluorescence correlation spectroscopy. J Mol Biol 298:677–689

Wachsmuth M, Weidemann T, Muller G, Hoffmann-Rohrer UW, Knoch TA, Waldeck W, Langowski J (2003) Analyzing intracellular binding and diffusion with continuous fluorescence photobleaching. Biophys J 84:3353–3363

Wachsmuth M, Caudron-Herger M, Rippe K (2008) Genome organization: balancing stability and plasticity. Biochim Biophys Acta 1783:2061–2079